IOP Conf. Series: Materials Science and Engineering **279** (2017) 012018 doi:10.1088/1757-899X/279/1/012018

Measurement of a Conduction Cooled Nb_3Sn Racetrack Coil

HS Kim[1], C Kovacs[1], J Rochester[1, 3], MD Sumption[1], M Tomsic[2], X Peng[2], D Doll[2]

[1] Department of Materials Science and Engineering, The Ohio State University, Columbus, Ohio 43210, USA
[2] Hyper Tech Research Incorporated, 539 Industrial Mile Road, Columbus, Ohio 43228, USA
[3] Author to whom any correspondence should be addressed. Electronic mail: rochester.11@osu.edu.

Abstract. Use of superconducting coils for wind turbines and electric aircraft is of interest because of the potential for high power density and weight reduction. Here we test a racetrack coil developed as a proof-of-concept for cryogen-free superconducting motors and generators. The coil was wound with 1209 m of 0.7-mm-diameter insulated tube-type Nb_3Sn wire. The coil was epoxy-impregnated, instrumented, covered with numerous layers of aluminized mylar insulation, and inserted vertically into a dewar. The system was cooled to 4.2 K, and a few inches of liquid helium was allowed to collect at the bottom of the dewar but below the coil. The coil was cooled by conduction via copper cooling bars were attached to the coil but also were immersed in the liquid helium at their lower ends. Several current tests were performed on the coil, initially in voltage mode, and one run in current mode. The maximum coil I_c at 4.2 K was 480 A, generating 3.06 T at the surface of the coil. The coil met the design targets with a noticeable margin.

1. Introduction

Superconducting motors and generators can have a much higher power density than their conventional counterparts. Such a high power density is an advantage for offshore wind turbines, where the size of the nacelle and tower are important cost factors [1-4]. For all-electric aircraft, higher power density and higher power per unit weight are the driving factors for the consideration of superconducting motors and generators [5-14]. This is enabled by superconducting machines because the superconducting windings can achieve magnetic fields above those of conventional windings, and energy density goes as the square of the field. For superconducting generators, some designs have superconducting rotors (inside), but conventional stators (surrounding the rotor). However, for fully cryogenic designs both the rotor and stator are superconducting. In these designs, the rotors generate field experienced by the stators and the stators are exposed to relatively high dB/dt, which leads to potentially large losses in the superconductor. A new design by Haran [15] uses field coils which surround a rotating induction coil. The induction coil is Cu, but the field coils are made from either Nb_3Sn or YBCO, and generate high fields, about 6-8 T in present designs. This large value leads to very high power densities, while keeping the losses relatively small, since the superconductors only experience a ripple field. Presently, Nb_3Sn is the more affordable option, and leads to very high power density designs.

The design for this machine calls for a set of racetrack-like windings placed to form a cylindrical field winding in side of which the induction coils rotate. In a previous paper [15], a design for one of these Nb_3Sn racetrack coils was given, along with field and strain modelling, and the coil construction

Table 1. Wire and coil specifications

Coil Material	
Former	Copper
Outer cover	316 stainless steel
Coil Parameters	
Winding pack Length	618.1 mm
Winding Pack Height	70.7 mm
Winding Pack Width	9.5mm
No. Turns	956.75
Total Conductor Length	1209 meters
Turns/layer	11
No. Layers	87
Wire	
Strand	Nb_3Sn, tracer number 3635
Insulation	s-glass
Number of Filaments	180
OD bare wire	0.7 mm
OD with insulation	0.8 mm
Non-Cu	46.5%
Heat Treatment	625C/120 h, vacuum

and winding was described. In this paper, we describe the test results on that coil, including current and field measurements at the target temperature as well as at higher temperatures.

In the final machine as designed, the system would use cryocoolers with the coil conduction cooled using thermal straps. In this work, we use conduction cooling, but for simplicity use a liquid helium reservoir as the cooling basin connected to the cooling straps, rather than a cryocooler. Nevertheless,

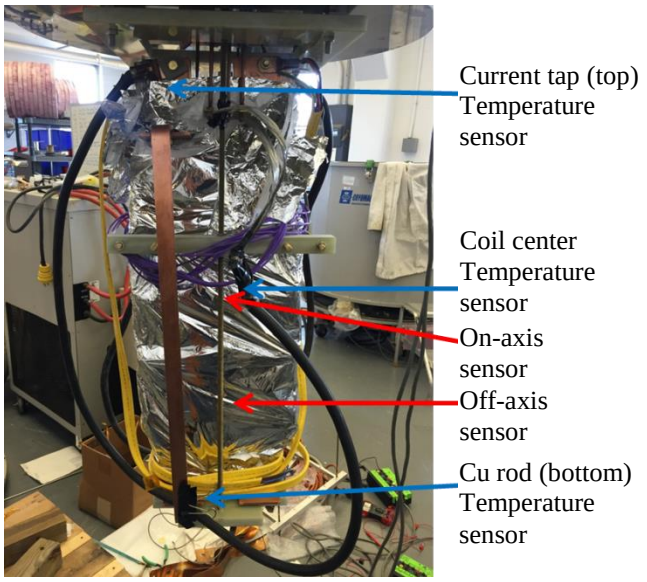

Figure 1. View of the coil instrumentation. Shown here are the three temperature sensors: one each at the current tap, coil center, and lower end of the Cu rod; as well as the two Hall sensors: one on-axis and one off-axis.

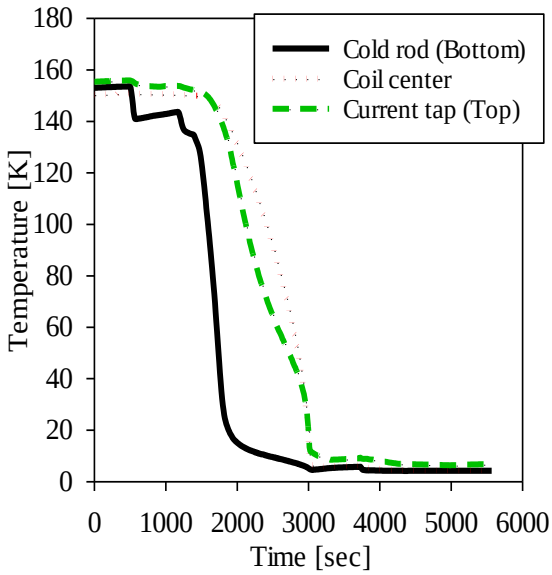

Figure 2. Temperature at each sensor during cooldown

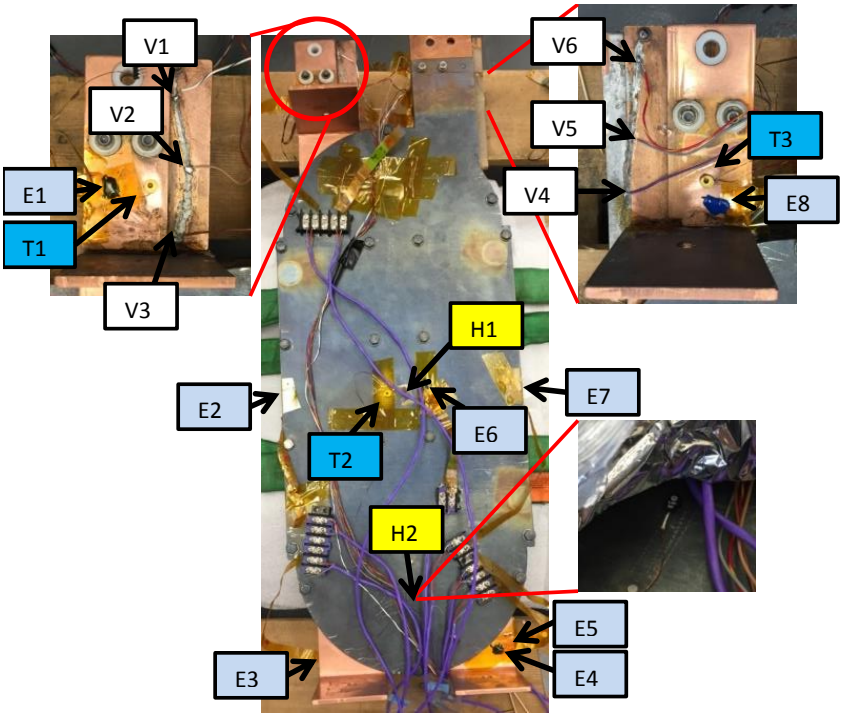

Figure 3. Location of instrumentation on the coil. Locations marked "V" notate voltage taps; "H", Hall sensors; "T", Cernox temperature sensors; and "E", Type-E thermocouples.

we are able to see the performance of the coil in conduction cooled mode, as well as the temperature gradient of the coil.

The coil measured here is the one which was modelled and described previously in [15]. Herein we report the results from the successful manufacture and testing of a prototype coil.

2. Manufacture

2.1. Conductor

The conductor (strand 3635), a tube-type strand manufactured by Hyper Tech Research, Inc. has 0.7 mm OD before insulation and contains 180 superconducting filaments. The filament size was 35 μm and the non-Cu area fraction was 46.5%. Pure Cu was used as the interfilamentary matrix. The wire was insulated with s-glass before winding.

2.2. Coil Winding

The coil was wound counter-clockwise with 1209 m of wire, with 11 turns per layer and 956.75 turns in total. The winding pack had a length of 618.1 mm, a height of 70.7 mm, and width of 9.5 mm. Actual winding payoff tension was maintained at 4.95 lbs. (nominal 5 lbs.).

After winding, the coil was heat treated in vacuum at 625°C for 120 hrs plus ramp-up and cool-down. Current leads were soldered with 40/60 Pb-Sn solder. The coil was then impregnated by vacuum infusion with epoxy at a pressure of 710 Torr, with flow duration of 7 hours and curing time of 24 hours. The epoxy was cured by heating tape with blanket at 80-90 °C.

2.3. Instrumentation

Measurements were enabled by the attachment of sensors to the coil (refer to Figures 1 and 3). Three Cernox temperature sensors were used; one at the current leads at the top, one at the center point of the coil, and one at the bottom end of the Cu support rods. Two Hall sensors were attached for magnetic flux measurement: one on-axis, and one off-axis at the point of maximum magnetic field. Several

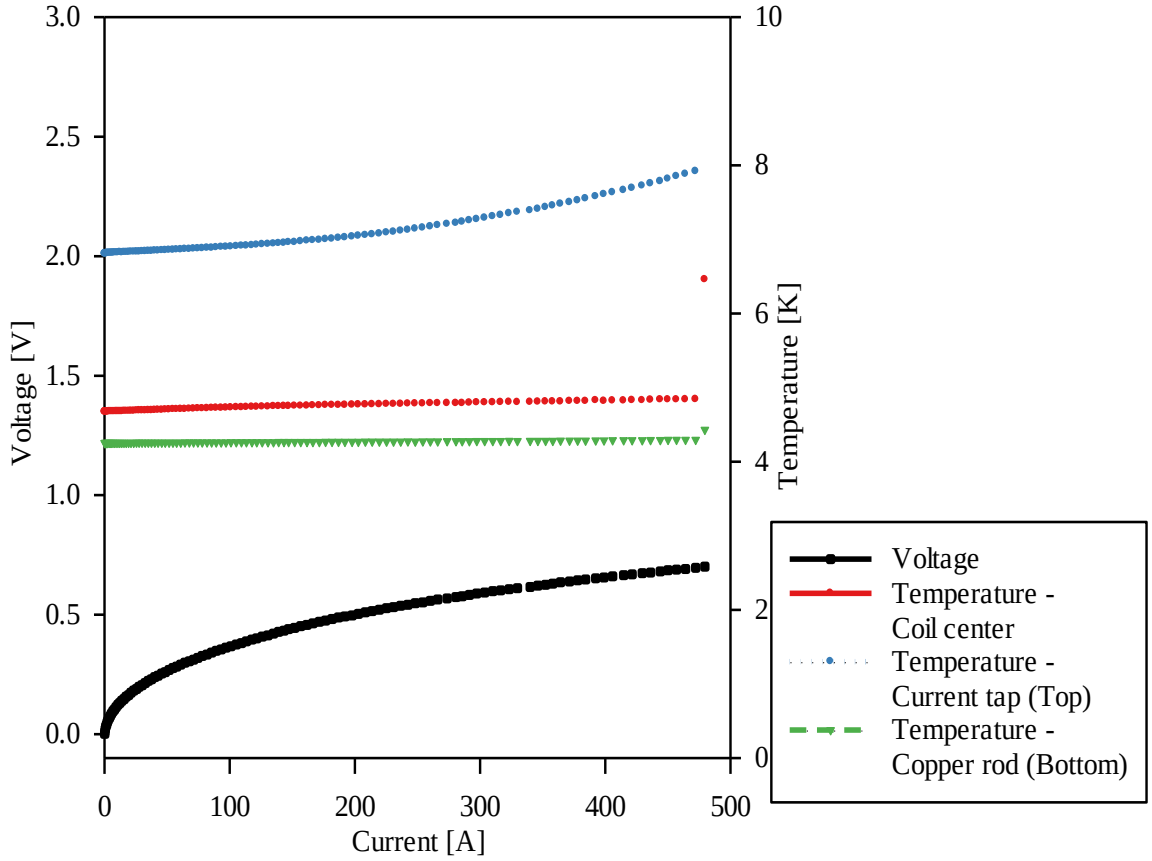

Figure 4. Current vs voltage and temperature in voltage mode (Run 4)

Type-E thermocouples were attached using Stycast 2850FT and insulated from the coil using thin cigarette paper. Voltage taps were also attached to the coil at intervals.

3. Coil Setup and Cooldown

The coil was mounted vertically in a dewar, sitting on a G10 plate which hangs on threaded rods from the top flange of the dewar. Insulated copper current leads ran from the top of the dewar, down into the liquid helium (just a few inches at the bottom of the dewar, below the coil itself) and then back up to the coil. The coil was covered with multilayer insulation to reduce radiative and convective heat transfer into the coil. The coil itself has a Cu former, with Cu cooling flanges which extend out the bottom of the coil; these flanges also serve in this instance as the feet of the coil, which rest on the G10 plate. An additional pair of Cu busbars runs to the top of the dewar (once can be seen). In addition, a dedicated set of flexible copper cables preferentially cool the leads.

At the start of the measurement, the coil was placed in the dewar and liquid nitrogen was injected slowly into the bottom of the dewar, cooling the coil overnight. The nitrogen was allowed to boil off before beginning the liquid helium fill.

After cooling, a few inches of liquid helium were allowed to accumulate at the bottom of the dewar, below the coil. The helium cooled the “feet” of the dewar, as well as the busbar, and these cooled the coil by conduction. The lowest temperatures achieved were 4.21 K at the coil bottom, 4.49 K at the coil center, and 6.46 K at the coil top (top of current lead). This gives a temperature difference across the coil of 2.25 K.

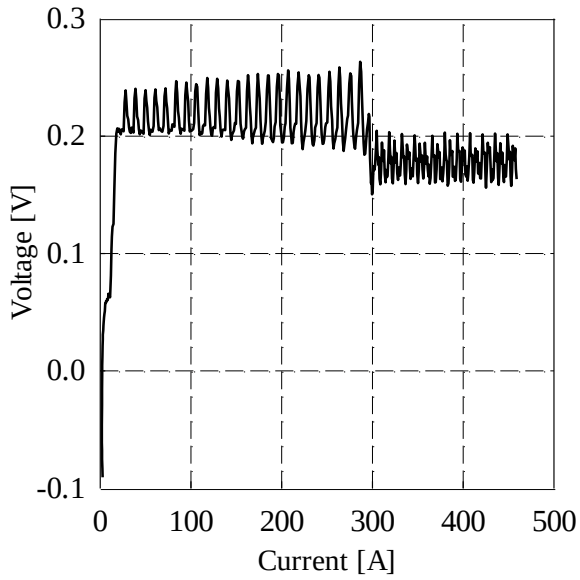

Figure 5. *I-V* data at 4.2 K in current mode

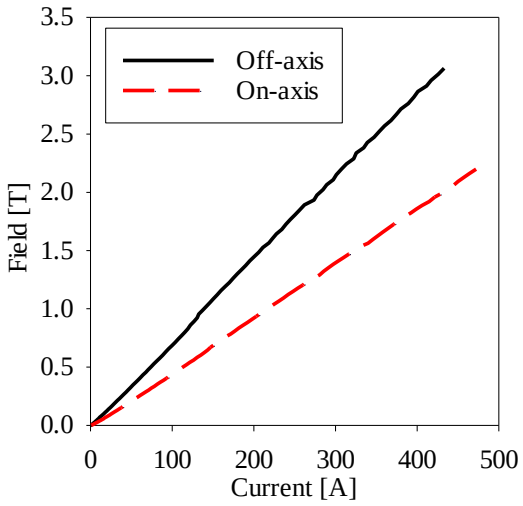

Figure 6. Field (*B*) vs current (*I*) at 4.2 K

Table 2. Critical/quench current of coil, and maximum field at 4.2 K

Run (#)	I_c, I_q [A]	Max Field [T] On-axis	Max Field [T] Off-axis
1	437	2.00	-
2	440	-	3.06
3	459	-	-
4	480	2.20	-

Table 3. Critical/quench current of coil and maximum field at various temperatures

Run (#)	Coil Temp. [K]	I_c, I_q [A]	Max Field [T] On-axis
5	5.56	457	2.09
6	8.02	384	1.75
7	10.83	265	1.20

4. Experiment

After the initial cool down, several current runs were performed. Initially the current was applied using voltage mode. It is a very safe way to run the magnet and is done to prevent the possibility of overvoltage during the run. The *I* vs *V* and *T* curve for the final run at 4.2 K (after some positive training of the coil) is shown in Figure 4. The voltage is not zero because it has an inductive component (we are measuring a magnet). The curves are not flat with an offset because the ramp rate changes during measurement as an artifact of the fact that we use voltage mode. The voltage ramping rate was 0.01 V/s, and the average current ramping rate above 400 A was approximately 1.1 A/s. The maximum take-off voltage trigger was set at 1 V. We can see that the temperature of the coil rises slightly for the coil end near the current taps; this is to be expected for a cryocooled coil unless very high additional cooling is present. All runs were fairly similar, although some positive training was seen. The transition was by quench, again not unexpected for an LTS coil running at high currents to I_c in conduction cooled mode.

The next step was a measurement of the coil in current mode. The benefit of this is that it provides a flat *I-V* curve, although that comes with an inductive voltage offset. The *I-V* curve for this run is shown in Figure 5. Current was applied with an initial ramping rate of 1 A/s, which was reduced to 0.8 A/s near 300 A. This reduction in current ramp rate explains the change in noise and inductive offset at 300 A. The maximum take-off voltage trigger was set at 300 mV.

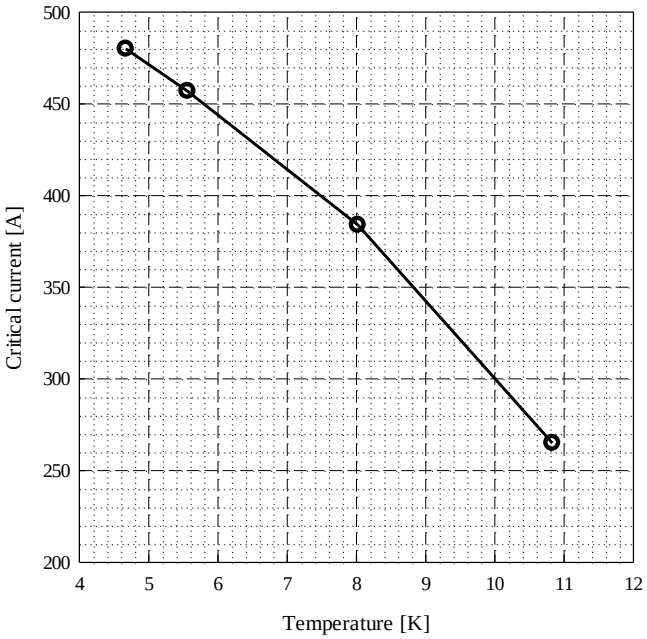

Figure 7. Critical current vs temperature of coil

The coil showed some positive training, but the best values obtained are shown in Table 2. The highest I_c was 480 A. This is above the target current of 435 A, with some margin. There is also a temperature margin, since the top portion of the coil was at 7.9 K at transition (see below). The target B (at the highest spot on the coil exterior) was expected to be 3 T at 435 A, and that is consistent with our measurement of 3.06 T at 440 A.

We note that the on-axis (H1, Figure 3) and maximum (H2, Figure 3) magnetic fields could not be measured simultaneously. They were measured on Run #4 and Run #2, respectively. The maximum on-axis field was measured at 480 A, while the maximum off-axis field was measured at 440 A (see Figure 6).

After the run in current mode, further voltage mode runs were performed to measure I_c as a function of temperature. Figure 7 shows the coil critical current as a function of temperature at the coil bottom. It should be kept in mind that the temperature at the top of the coil was about 2.5-3 K higher than at the bottom. This would suggest that the actual coil I_c at 4.2 K is closer to 550 A.

5. Summary

A Nb_3Sn coil was fabricated, cooled, and tested. A small amount of liquid helium below the coil was used as the cold reservoir with the coil cooled by conduction through the cooling legs. The operational current target of $I = 435$ A was achieved, with both current (45 A) and temperature (3.8 K) margin. The field values reached 3 T at the outer can of the coil, as expected by modelling. The coil met the needed targets for the winding design with a noticeable margin.

References

[1] A. B. Abrahamsen, N. Mijatovic, E. Seiler, T. Zirngibl, C. Træholt, P.B. Nørgard, N.F . Pedersen, N.H. Andersen, and J. Østergard, "Superconducting wind turbine generators", Supercond. Sci. Technol. 23 (2010) 034019.

[2] B. B. Jensen, N. Mijatovic, , and A. B. Abrahamsen, "Development of superconducting wind turbine generators", Journal of Renewable and Sustainable Energy 5, (2013) 023137; doi: 10.1063/1.4801449

[3] H. Ohsaki, L. Quéval, and Y. Terao, "Design and Characteristic Analysis of 10 MW Class

Superconducting Wind Turbine Generators with Different Types of Stator and Rotor Configurations", IEEE Trans Appl. Supercond. (2013) 398.

[4] X. Song and B. Bech, "Design Study of Fully Superconducting Wind Turbine Generators", IEEE Trans. Appl. Supercond. 25 (2015) 5203605

[5] R.H. Jansen, G.V. Brown, JL. Felder, K.P. Duffy, "Turboelectric Aircraft Drive Key Performance Parameters and Functional Requirements", Proc. Of Propulsion and Energy 2015, At Orlando, Florida

[6] P. Gemin, T. Kupiszewski, A. Radun, Y Pan, R. Lai, D. Zhang, R. Wang, X. Wu, Y. Jiang, S. Galioto, K. Haran, W. Premerlani, J. Bray, and A. Caiafa, "Architecture, Voltage and Components for a Turboelectric Distributed Propulsion Electric Grid (AVC-TeDP), NASA Technical report, NASA/CR—2015-218713.

[7] C. A. Luongo, P. J. Masson, T. Nam, D. Mavris, H. D. Kim, G. V. Brown, M. Waters, and D. Hall, "Next Generation More-Electric Aircraft: A Potential Application for HTS Superconductors", IEEE Trans. Appl. Supercond. 19 (2009) 1055.

[8] J. L. Felder, G. V. Brown, H.D. Kim, J. Chu, "Turboelectric Distributed Propulsion in a Hybrid Wing Body Aircraft", Proceedings of the XX International Symposium on Air Breathing Engines 2011 : (ISABE 2011) : Gothenburg, Sweden, 12-16 September, 2011, pp. 1340

[9] P. J. Masson, G. V. Brown, D. S. Soban and C. A. Luongo, "HTS machines as enabling technology for all-electric airborne vehicles", Supercond. Sci. Technol. 20 (2007) 748–756 doi:10.1088/0953-2048/20/8/005

[10] F. Berg, J. Palmer, P. Miller, M. Husband, and G. Dodds, "HTS Electrical System for a Distributed Propulsion Aircraft", IEEE Trans. Appl. Supercond. 25 (2015) 5202705

[11] F. Berg, J. Palmer, P. Miller, and G. Dodds, "HTS System and Component Targets for a Distributed Aircraft Propulsion System", IEEE Trans. Appl. Supercon. 27 (2017) 3600307

[12] T. Haugan, "Development of Superconducting and Cryogenic Power Systems and Impact for Aircraft Propulsion", Presentation, Energy Materials and Applications, Orlando FL, 25 Jan 2013.

[13] P.N. Barnes , M.D. Sumption, G.L. Rhoads, "Review of high power density superconducting generators: Present state and prospects for incorporating YBCO windings", Cryogenics 45 (2005) 670–686

[14] P.N. Barnes, G.L. Rhoads, J.C. Tolliver, M.D. Sumption, and K.W. Schmaeman, "Compact, Lightweight, Superconducting Power Generators", IEEE Transactions on Magnetics 41 268-273 (2005).

[15] D. Loder, R. Sanchez, M. Feddersen, K. Haran, M. Sumption, M. Tomsic, Y. Jinji and D. Doll, "A Conduction Cooled Nb_3Sn Racetrack Coil: Design, Construction, and Testing," 2016 IEEE Power and Energy Conference at Illinois (PECI), 2016.